Nucl Eng Technol 47 (2015) 804–813

Available online at www.sciencedirect.com

ScienceDirect

journal homepage: http://www.journals.elsevier.com/nuclear-engineering-and-technology/



Original Article

AN IMPROVED ELECTRICAL-CONDUCTANCE SENSOR FOR VOID-FRACTION MEASUREMENT IN A HORIZONTAL PIPE

MIN SEOK KO [a], *BO AN LEE* [b], *WOO YOUN WON* [c], *YEON GUN LEE* [c], *DONG WOOK JERNG* [a,d], *and SIN KIM* [d,*]

[a] *Nuclear Safety Research Center, Chung-Ang University, Heukseok-dong, Dongjak-gu, Seoul 156-756, Korea*
[b] *Institute for Nuclear Science and Technology, Jeju National University, Arail-dong, Jeju-si, Jeju-do 690-756, Korea*
[c] *Department of Nuclear and Energy Engineering, Jeju National University, Arail-dong, Jeju-si, Jeju-do 690-756, Korea*
[d] *School of Energy Systems Engineering, Chung-Ang University, Heukseok-dong, Dongjak-gu, Seoul 156-756, Korea*

ARTICLE INFO

Article history:
Received 14 April 2015
Received in revised form
18 June 2015
Accepted 29 June 2015
Available online 3 October 2015

Keywords:
Conductance Sensor
Flow Pattern
Void Fraction
Wire-mesh Sensor

ABSTRACT

The electrical-impedance method has been widely used for void-fraction measurement in two-phase flow due to its many favorable features. In the impedance method, the response characteristics of the electrical signal heavily depend upon flow pattern, as well as phasic volume. Thus, information on the flow pattern should be given for reliable void-fraction measurement. This study proposes an improved electrical-conductance sensor composed of a three-electrode set of adjacent and opposite electrodes. In the proposed sensor, conductance readings are directly converted into the flow pattern through a specified criterion and are consecutively used to estimate the corresponding void fraction. Since the flow pattern and the void fraction are evaluated by reading conductance measurements, complexity of data processing can be significantly reduced and real-time information provided. Before actual applications, several numerical calculations are performed to optimize electrode and insulator sizes, and optimal design is verified by static experiments. Finally, the proposed sensor is applied for air-water two-phase flow in a horizontal loop with a 40-mm inner diameter and a 5-m length, and its measurement results are compared with those of a wire-mesh sensor.

Copyright © 2015, Published by Elsevier Korea LLC on behalf of Korean Nuclear Society.

1. Introduction

Gas-liquid two-phase flows are frequently encountered phenomena in various engineering fields, such as chemical, oil, and nuclear industries. Specifically, the void fraction in two-phase flows is one of the key parameters associated with system analyses and designs. For this reason, many techniques, including nuclear sources [1,2], optical [3], electrical impedance [4,5], and wire-mesh tomography, have been proposed [6,7]. Among these instruments, the electrical-impedance technique has a variety of advantages, such as easy implementation, no intrusiveness of flow field, no

* *Corresponding author.*
E-mail address: sinkim@cau.ac.kr (S. Kim).

This is an Open Access article distributed under the terms of the Creative Commons Attribution Non-Commercial License (http://creativecommons.org/licenses/by-nc/3.0) which permits unrestricted non-commercial use, distribution, and reproduction in any medium, provided the original work is properly cited.

http://dx.doi.org/10.1016/j.net.2015.06.015
1738-5733/Copyright © 2015, Published by Elsevier Korea LLC on behalf of Korean Nuclear Society.

radiation, and convenient mobility. Owing to these merits, the electrical-impedance technique has received much attention and various designs of electrical-impedance sensors have been proposed.

One of the most common shapes is the plate-type sensor. In this sensor, pairs of concave electrodes are arranged on the inner or outer walls of the pipe and measure the electrical impedance between them [8–12]. The ring-type sensor is another common type. For this sensor, two or more ring electrodes covering the whole pipe circumference are arranged along the pipe and measure the electrical impedance [13–16]. Other types include helical [17,18], internal [19], and wire electrodes [20].

In the electrical-impedance sensor, the electrical signal depends on the flow structure, as well as the void fraction. For this reason, the electrical responses to a given void fraction differ according to the flow pattern. Thus, information on the flow pattern should be given in order to achieve reliable void-fraction measurement.

The present study proposes an improved electrical-conductance sensor for void-fraction measurement, which is applicable for practical two-phase flows in horizontal pipes. The proposed sensor is composed of a three-electrode set of adjacent and opposite electrodes. In the sensor, the conductance readings in the electrode pairs are directly converted into the flow pattern through a specified criterion for flow-pattern classification, and the void fractions are successively evaluated from a relevant calibration curve.

The idea of the proposed method is similar to the work done by De Kerpel et al. [12]. Since the flow pattern is classified by the measured-conductance signal, unlike the study of De Kerpel et al. [12], which used several statistical parameters, the burden of data processing can be reduced and both the real-time information on the flow pattern and the void fraction can be provided.

Prior to the real applications of the proposed approach, several numerical calculations based on the finite-element method (FEM) are performed in order to optimize the electrode and insulator sizes in terms of the sensor linearity and these are verified in comparison with static experiments. Finally, the sensor system is applied for a horizontal flow loop with a 40-mm inner diameter and a 5-m length, and its measured performance for the void fraction is compared with that of a wire-mesh sensor system.

2. Numerical analysis for sensor optimization

Let us consider stratified flow and annular flow through the conductance sensor, as shown in Fig. 1. In both cases, the electrical conductivities of the gas and liquid phases are denoted by σ_g and σ_ℓ, respectively. Two electrodes with an identical size (electrode A and B) are separated from an insulator by the angle θ_1 in the bottom and from the electrode C and two insulator gaps by the angles θ_2 and θ_3 in the top of the sensor.

In each phase, the potential distribution can be described by the following Laplace equations:

$$\nabla \cdot \sigma_g \nabla u_g = 0 \quad \text{for the gas phase} \tag{1A}$$

$$\nabla \cdot \sigma_\ell \nabla u_\ell = 0 \quad \text{for the liquid phase} \tag{1B}$$

where u_g and u_ℓ represent the potential distribution to be determined for each phase.

If the electrical current is I, the electrical conductance can be written as $G = I/\Delta V$. Here, ΔV is the voltage difference applied to a pair of opposite electrodes (electrode A and B in Fig. 1). For convenience, let us now define the dimensionless conductance as:

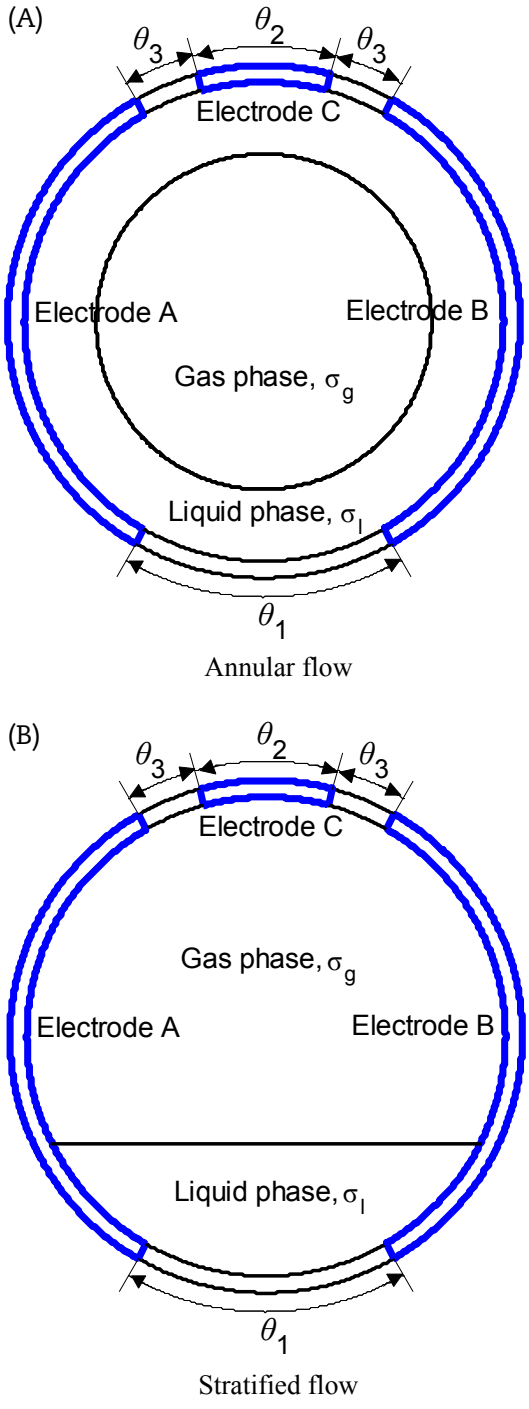


Fig. 1 – Stratified and annular flow through the conductance sensor.

$$G^*_{opp} = \frac{G}{G_\ell}. \quad (2)$$

Here, G_ℓ is the conductance value in the opposite electrodes for the sensor measured when the flow channel is filled only with liquid ($\alpha = 0$) and G for a certain two-phase flow. Eq. (2) indicates that G^*_{opp} is minimum $G^*_{opp} = 0$ at $\alpha = 1$, and maximum $G^*_{opp} = 1$ at $\alpha = 0$.

To solve the governing equations in a three dimensional computational domain, COMSOL Multiphysics (ALTSOFT, Seoul, Korea) based on the FEM was employed. Considering air-water two-phase flow applications, the conductivity values of the gas and liquid phases have been set to $\sigma_g = 0\ m^{-1}\Omega^{-1}$ and $\sigma_\ell = 0.005\ m^{-1}\Omega^{-1}$, respectively. The electrical conductivity for each electrode volume was $\sigma_e = 10^6\ m^{-1}\Omega^{-1}$ and for the insulators was $\sigma_i = 0\ m^{-1}\Omega^{-1}$. The magnitude of the voltage difference applied to the opposite electrodes was set to 1V. The insulation conditions were applied for all boundaries, except activated electrodes. Each electrode and insulator angle ranging from 0.1 rad to 0.5 rad by 0.1 rad was considered. The full range of the void fractions ($\alpha = 0 \sim 1.0$) for stratified flow were taken into account, while for annular flow, the void fractions ranging from 0.5 to 1.0 ($\alpha = 0.5 \sim 1.0$) were tested [21].

To find the optimal electrode and insulator sizes, the following nonlinearity error was introduced:

$$\text{Nonlinearity error} = \left|G^*_{linear} - G^*_{opp}\right|_{\max} \times 100\ (\%), \quad (3)$$

where G^*_{linear} is the linear-conductance response ($G^*_{linear} = \alpha$) and G^*_{opp} is the calculated dimensionless conductance given in Eq. (2).

Figs. 2–4 show the numerical trends of the nonlinearity errors for θ_1, θ_2, and θ_3, respectively. When θ_1 and θ_3 are small for a given θ_2 in annular flow, the electric-field distribution is essentially distorted near the insulator gaps. This causes particular increase in the nonlinearity error for the cases where the void fraction is < 0.8 [22]. As θ_1 and θ_3 increase, the electric-field distribution becomes more uniform across the sensor and the sensor linearity is enhanced

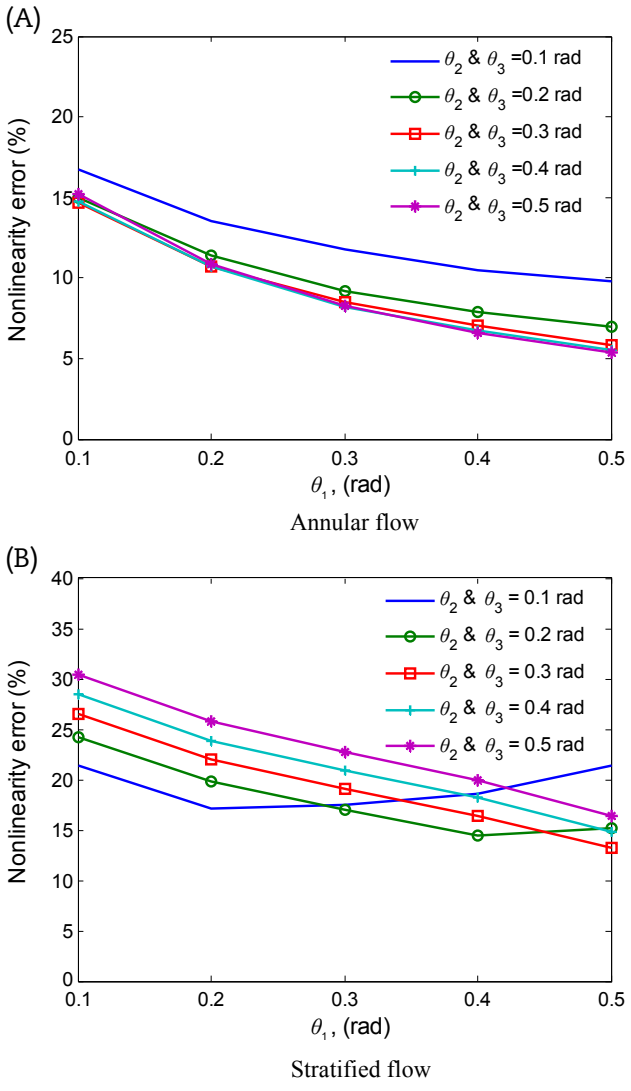


Fig. 2 – The nonlinearity errors for various θ_1 values.

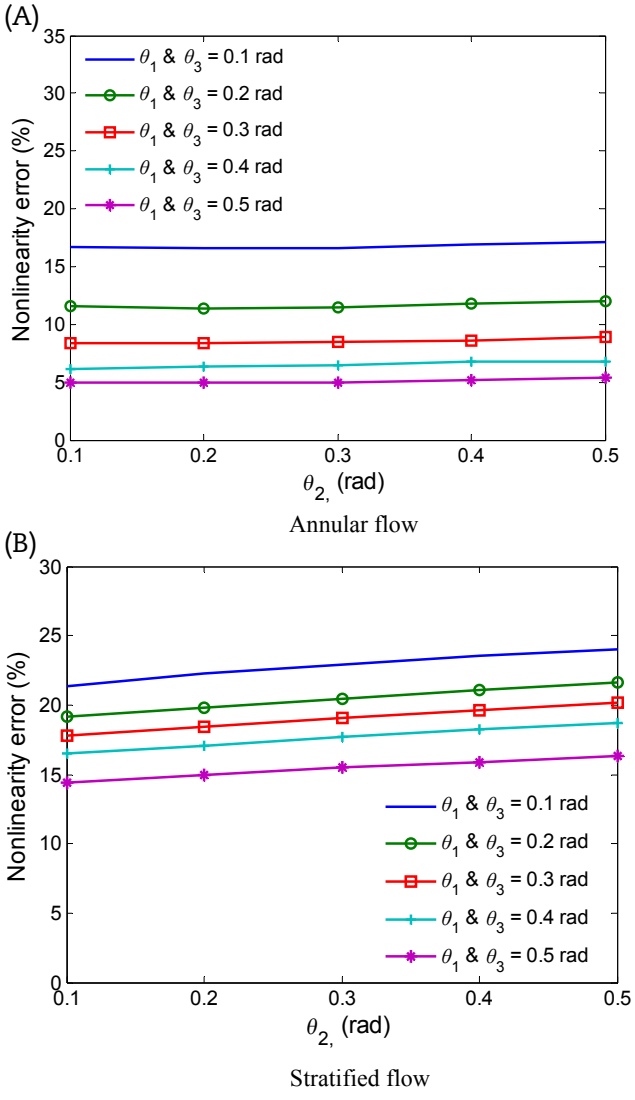


Fig. 3 – The nonlinearity errors for various θ_2 values

(Figs. 2A and 4A). In annular flow, the effects of θ_2 on G and G_ℓ are comparable, hence, its effects on sensor linearity are negligibly small (Fig 3A).

The overall trends of the nonlinearity errors for stratified flow, however, are somewhat different, in particular for θ_2 and θ_3. These are mainly due to differences in interfacial structures of annular and stratified flow. In other words, unlike the annular flow cases where the whole circumference of the sensor is in contact with the conductive liquid film, only oppositely installed electrodes A and B have partial contact with conductive liquid in stratified flow. For this reason, the dependence of G on θ_2 is significantly reduced, while G_ℓ still depends upon it. In this flow pattern, therefore, the effects of θ_2 on the conductance responses, G and G_ℓ, are no longer comparable and θ_2 affects the sensor linearity (Fig. 3B). It is also interesting to note that due to the effects of θ_2, the nonlinearity errors show some minimum points, unlike annular flow (Figs. 2B and 4B). Similarly, when the upper insulator size, θ_3, increases for a given θ_1 and θ_2, the conductance response for the reference G_ℓ decreases, while G is almost constant because G does not depend upon θ_3, as previously mentioned. This leads to increases in G^*_{opp} and eventually to deterioration in the sensor linearity (Fig. 4B).

To summarize the numerical results, it is shown that sensor linearity is optimized when θ_1, θ_2, and θ_3 are 0.5 rad, 0.2 rad, and 0.3 rad, respectively. In this geometric arrangement, the nonlinearity errors for annular flow and stratified flow are 5.7% and 12.7%, respectively. Also, it should be noted that due to the gap on the bottom, there is a small dead zone that is not detecting the small liquid fraction. However, the gap size is $\theta_1 = 0.5$ rad, which corresponds to a 0.3% liquid fraction.

3. Sensor system setup and verification of numerical results

Several static experiments were performed to verify the numerical results for the sensor nonlinearity discussed in the preceding section. A conductance sensor was fabricated following the dimensions determined in the numerical calculations. That is, the inner diameter of the sensor was 40 mm and three electrodes with 2-mm thickness were flush mounted on the inner wall of the pipe. The insulator angle on the bottom was $\theta_1 = 0.5$ rad and those for the insulator on the top and the electrode, C, were $\theta_2 = 0.2$ rad and $\theta_3 = 0.3$ rad, respectively.

For measurement, an Agilent 4284A LCR meter (Agilent, Santa Clara, CA, USA) was used to provide voltages to the electrodes and a NI PXI-2536 (National Instruments, Seoul, Korea) was employed to shift the voltage sources from the adjacent electrodes (electrodes A and C) to the opposite pair of electrodes (electrode A and B) and vice versa. Also, a NI PXIe-6368 (National Instruments) was used for data sampling. These instruments were connected with the conductance sensor through the cables via NI PXIe-1062Q (National Instruments). Fig. 5 and Table 1 provide the connections and the specifications of the measurement instruments involved in the experiments, respectively.

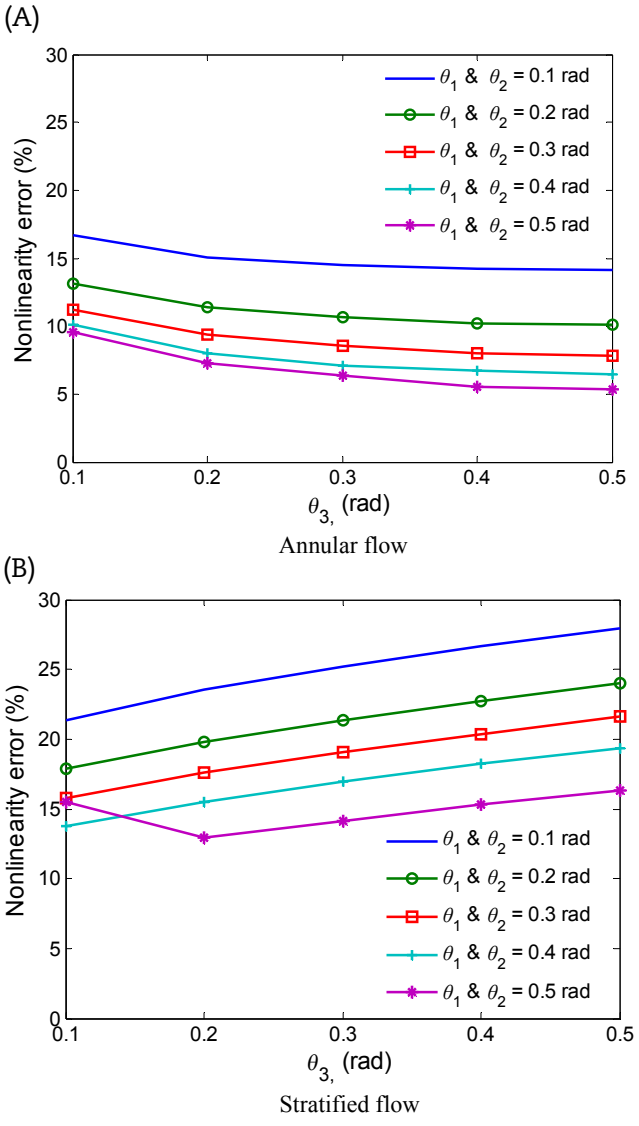


Fig. 4 – The nonlinearity errors for various θ_3 values.

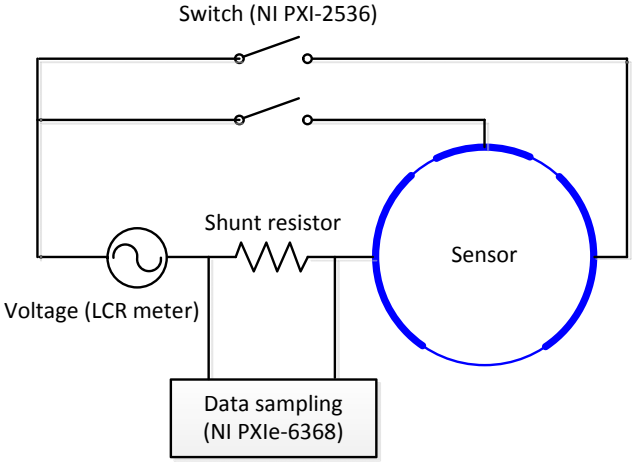


Fig. 5 – Schematic diagram of sensor system.

Table 1 – Specifications of measurement instruments used for experiments.

Instruments	Accuracy	Signal range	Time definition
Agilent 4284A LCR meter	0.05~0.5%	Up to 20 V with 1 MHz	N/A
NI PXI-2536	N/A	Up to ±12 V and 100 mA	50,000 cross-points/sec
NI PXIe-6368	1.5 mV for ±10 V range	Up to ±10 V	2,000,000 samples/channel

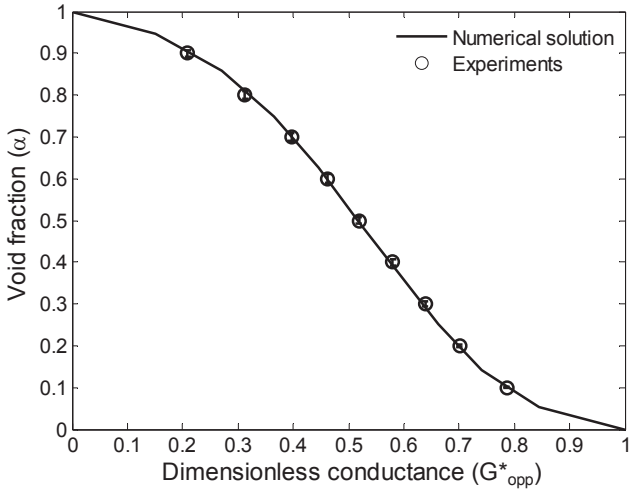


Fig. 6 – Comparison between numerical solutions and experimental results for stratified flow.

In the experiments, the applied voltage was set to 5 V with 10 kHz signal frequency to ensure that the impedance response became conductive [13–15] and the sampling frequency of 10,000/sec was used. The uncertainty of conductance measurement was evaluated by the error propagation as follows:

$$U_G = \pm\left[\left(\frac{\partial G}{\partial V}U_V\right)^2 + \left(\frac{\partial G}{\partial I}U_I\right)^2\right]^{1/2} \quad (4)$$

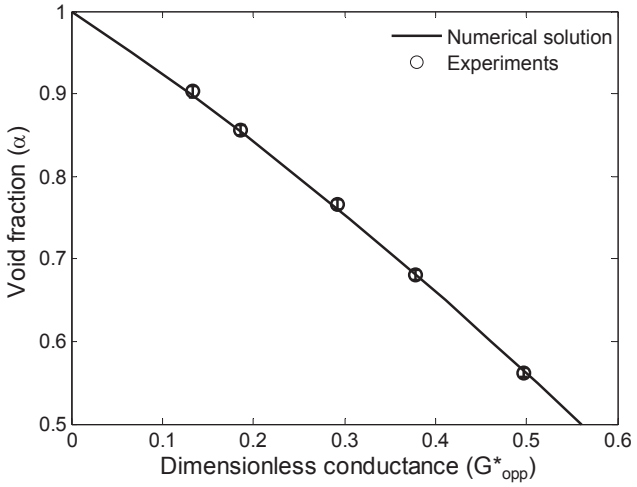


Fig. 7 – Comparison between numerical solutions and experimental results for annular flow.

where the first and second partial derivatives of the right hand side are given by:

$$\frac{\partial G}{\partial V} = \frac{-I}{V^2} \text{ and } \frac{\partial G}{\partial I} = \frac{1}{V} \quad (5)$$

The accuracy of the LCR meter was 0.1% (Table 1) and the applied voltage was 5 V, thus the first term of the right hand side in Eq. (4) can be neglected and the expression (4) is reduced to:

$$U_G = \pm\frac{U_I}{V}. \quad (6)$$

Since the data sampling instrument has the absolute accuracy of 1.5 mV (NI-PXIe 6368 in Table 1), the measurement uncertainty for electrical current can be estimated as $U_I \approx 15\ \mu A$ for a 100 Ω shunt resistor with 0.1% accuracy, and this consequently leads to $U_G \approx \pm 15\ \mu A/5V = \pm 3\ \mu\Omega^{-1}$.

The static experiments were performed with a horizontally-laying conductance sensor, which contained the specified volume of water for stratified flow and by inserting acryl rods into the sensor for annular flow. Here, the diameters of the acryl rods used for experiments were 30 mm, 33 mm, 35 mm, 37 mm, and 38 mm, corresponding to the void fractions 0.56, 0.68, 0.76, 0.86, and 0.9, respectively.

Figs. 6 and 7 show the comparison results between the numerical solutions and experimental data with uncertainties for stratified flow and annular flow, respectively. For both cases, the experimental results showed good agreement with numerical predictions. The nonlinearity errors for stratified flow and annular flow were ~12.0% and ~7.0%, respectively, which were comparable to those of the numerical calculations (12.7% for annular flow and 5.7% for stratified flow).

4. Proposed method for void-fraction measurement

The proposed method to measure the void fraction is mainly composed of two steps, as briefly mentioned in the Introduction section. In the first step, the flow pattern is identified using the conductance signal measured in all electrode pairs. Then, in the second step, the void fraction is estimated through the calibration curve for the flow pattern predetermined in the first step. Details are discussed in this section.

4.1. *Criteria for flow-pattern classification*

In this work, three flow patterns of horizontal pipes were considered: stratified, annular, and intermittent flow. In stratified flow, smooth or wavy interfaces were formed between the gas and liquid phases, and these were not in contact with the top of the pipe. For this flow pattern, hence, the

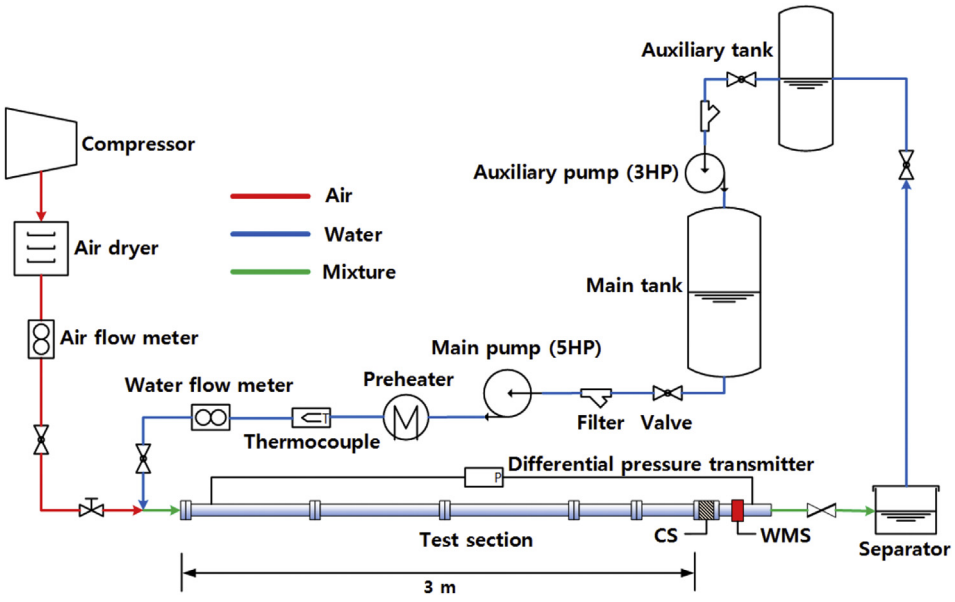


Fig. 8 – Schematic diagram of horizontal loop.

conductance signal in the adjacent electrodes A and C, G^*_{adj}, should be negligibly small. The static experiments indicated that G^*_{adj} was < 0.005 (0.5%) for this case ($G^*_{adj} < 0.005$). This value actually corresponds to the standard deviation of measurement data.

When the flow pattern changes from stratified to non-stratified flow, conductive liquid film, or liquid slug touches the top of the pipe. This obviously causes G^*_{adj} to become at least equal to or greater than the stratified-flow cases ($G^*_{adj} \geq 0.005$).

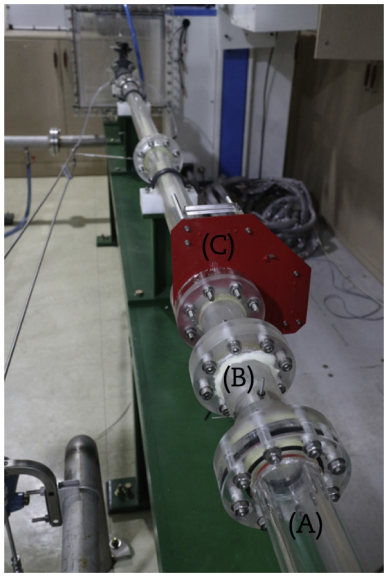


Fig. 9 – Photo of sensor installations: (A) Test section, (B) Conductance sensor, (C) Wire-mesh sensor.

Meanwhile, it was reported that the transition from stratified to intermittent flow occurred when the liquid level was > 0.5 for the pipe diameter [23]. This hydraulic criterion corresponds to $\sim G^*_{opp} > 0.51$, as indicated in Fig. 6. Similarly, Barnea [21] proposed that the minimum void fraction of annular flow in horizontal pipes was 0.76. This roughly gives rise to $G^*_{opp} < 0.3$, as shown in Fig. 7 (The actual criterion is $G^*_{opp} \leq 0.295$). Combining these two criteria, G^*_{opp} should be at least ≥ 0.3 for intermittent flow to occur ($G^*_{opp} \geq 0.3$).

The criteria for flow-pattern classification in this study are summarized as follows:

$$G^*_{adj} < 0.005 \text{ for stratified flow,} \tag{7A}$$

$$G^*_{adj} \geq 0.005 \text{ and } G^*_{opp} < 0.3 \text{ for annular flow,} \tag{7B}$$

$$G^*_{adj} \geq 0.005 \text{ and } G^*_{opp} \geq 0.3 \text{ for intermittent flow.} \tag{7C}$$

Table 2 – Test matrix for some selected flow conditions.

Case	j_l (m/s)	j_g (m/s)	Flow pattern
01	0.05	7.9	Stratified flow
02	0.1	7.7	Stratified flow
03	0.4	7.1	Intermittent flow
04	0.56	6.6	Intermittent flow
05	0.76	6.5	Intermittent flow
06	0.9	6.8	Intermittent flow
07		4.2	Intermittent flow
08		6.3	Intermittent flow
09	0.2	8.5	Intermittent flow
10		10.8	Intermittent flow
11		12.7	Intermittent flow
12		14.2	Intermittent flow

The above equations were driven for the sensor configuration providing better sensor linearity. However, these criteria can differ if the electrode and insulator gap angles change.

4.2. *Measurement of void fraction*

In the first measurement stage, the conductance signals, G^*, are measured in each electrode pair and the flow pattern is classified based on the criteria given in Eq. (7). Once the flow pattern is identified, in the next measurement stage, the void fraction is evaluated by interpolating the conductance measurement in the opposite electrode pair, G^*_{opp}, into a conductance-void fraction lookup table, which corresponds to Figs. 6 or 7. For intermittent flow, both numerical and experimental simulations are not straightforward due to the complexity of the interface. This work assumed that the intermittent flows belong to the stratified flows rather than the annular flows.

5. Experimental apparatus

5.1. *Horizontal loop*

The experiments were conducted using a horizontal flow loop at Jeju National University, Jeju. Korea. This loop was mainly composed of a main tank, main pump, preheater, air compressor, test section, separator, auxiliary tank, and pump. The acrylic test section had a 40-mm diameter and a ~5-m length. The proposed conductance sensor (CS) was placed at a distance of approximately 3 m away from the entrance ($L/D = 75$) and a wire-mesh sensor (WMS, WMS200) was installed near the sensor ($L/D = 80$). A schematic of the loop and a photograph of sensor installations are given in Figs. 8 and 9, respectively.

5.2. *Wire-mesh sensor*

A conductivity wire-mesh sensor was used to evaluate the performance of the proposed sensor. The wire-mesh sensor and electronic devices were designed by HZDR (Helmholtz-Zentrum Dresden-Rossendorf, Dresden, Germany). The wire-mesh sensor adopted in this study consisted of 16 transmitter and receiver wires that were perpendicularly arranged, giving a total of 256 crossing points. The thickness of the wires was 0.125 mm and each wire was separated by 2.5 mm. The separation distance between the transmitter and receiver layer was 1.4 mm. In the experiments, the wire-mesh sensor was installed approximately 20 cm away from the conductance sensor. For this separation distance, no electrical interference between the two sensor systems was observed in the static experiments.

In the wire-mesh sensor, the void fraction was evaluated assuming the linear relation between the measured voltage ratio and the void fraction [24]. This indicated that the output voltages for the test section filled with water and air were first measured. Then, those for arbitrary air–water two-phase flows were recorded. The ratios of these measured voltages were linearly converted into the local instantaneous void fraction.

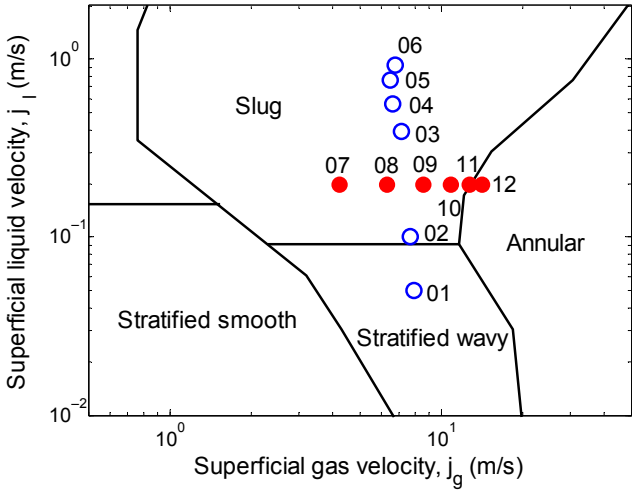


Fig. 10 – Some selected flow conditions on the flow regime map of Mandhane et al. (1974).

6. Experimental results and discussion

For the loop experiments, various superficial velocities ranging from 0.05 m/s to 1.2 m/s for water ($j_\ell = 0.05 \sim 1.2$ m/s) and from 0.8 m/s to 14.7 m/s for air ($j_g = 0.8 \sim 14.7$ m/s) were considered. Some selected flow conditions to be discussed here are given in Table 2, and these are illustrated on the experimental-flow pattern map of Mandhane et al. [25], as shown in Fig. 10.

In the experiments, the switch and sampling rates of the conductance sensor were set to 1,000/sec and 10,000/sec and the measurement frame of the wire-mesh sensor was set to 10,000/sec. These two sensor systems were synchronized by a customized clock box.

Fig. 11 and 12 show the comparison results between the conductance sensor (CS) and the wire-mesh sensor (WMS) for given experimental conditions.

When the superficial liquid velocity was low (Case 1), the void fraction signal was overall high and the conductance signals which meet the criterion (7B) or (7C) were not observed. As the superficial liquid velocity increased (Case 2), the void fraction decreased, but its fluctuation increased. For further increase of the superficial liquid velocity (Case 3), the conductance signals satisfying the criteria (7B) and (7C) finally appeared and the void fraction signal fluctuated more severely. As the superficial liquid velocity further increased (Cases 4–6), the frequency of the liquid slug occurrence significantly increased. Contrary to these trends, for increases in the superficial gas velocities (Cases 7–12), the interfacial waves were swept away by the gas phase and the liquid film formed around the wall of the sensor. As a result, the frequency of the liquid film formation considerably increased while the slugging frequency decreased.

The measurement results of the proposed sensor were generally in good agreement with the wire-mesh. Also, even though the approach for void-fraction measurement in intermittent flow in this study was simple (see *Measurement*

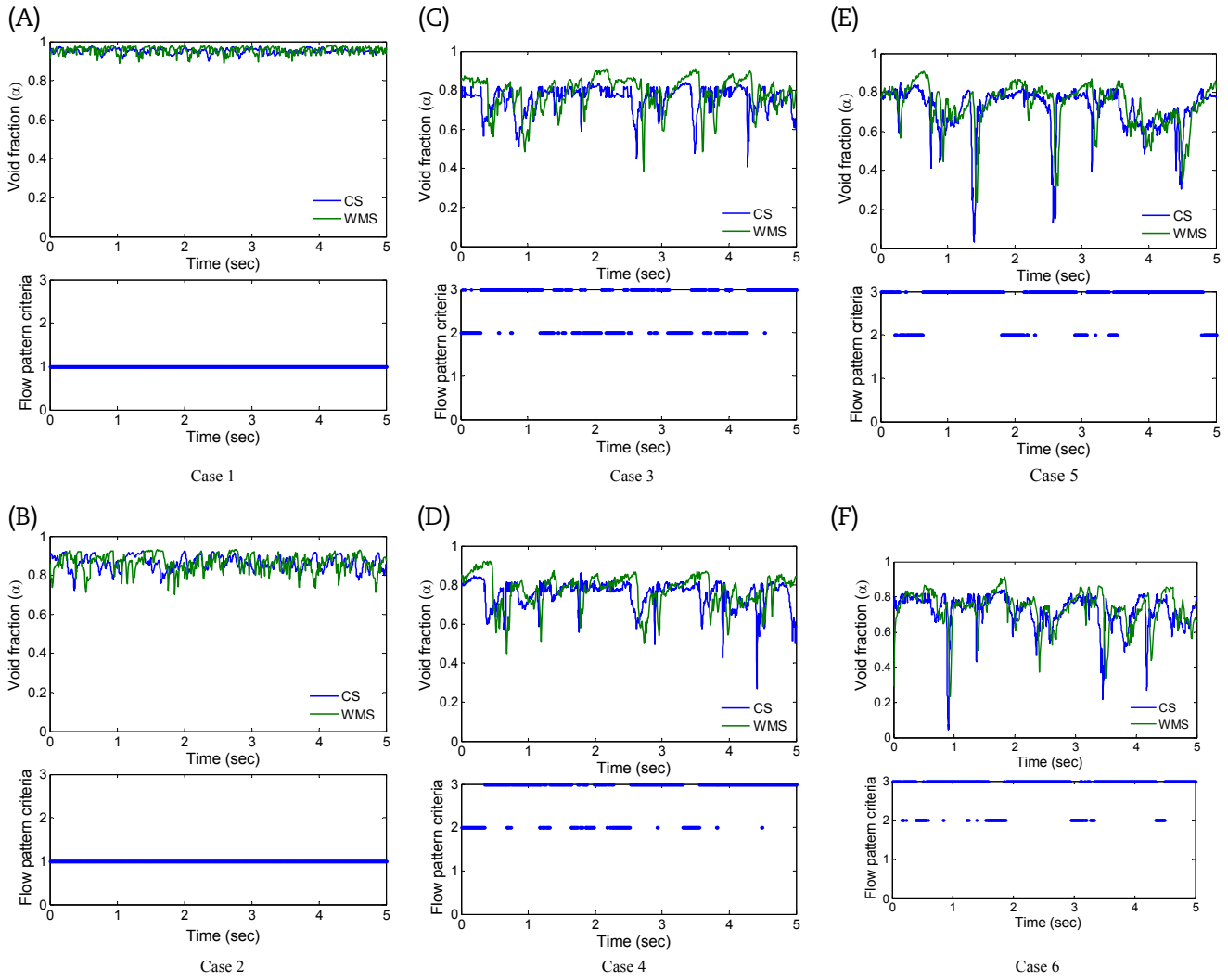


Fig. 11 – Comparison in instantaneous void fraction between CS and WMS for superficial liquid velocities. The numbers '1', '2', and '3' on the y axis of the bottom figures represent the flow pattern criteria (7A), (7B), and (7C), respectively.

of void fraction section), the comparison results showed its usefulness, as indicated in Cases 4–6 of Fig. 11. Fig. 13 shows the comparison results for the time-averaged void fraction. Very good agreements between the proposed sensor and the WMS were confirmed. For all flow-rate conditions, the maximum deviation between two instruments was 6.3%. However, it was observed that the void fractions in the proposed sensor were generally under compared to the WMS.

In the practical two-phase flows, the bubbles might be contained in the liquid phase or the liquid droplets might be suspended in the gas phase. In the WMS, these local phenomena could be measured to some extent, while the CS essentially has difficulties in detecting them due to its own mechanical structure and measurement modality. These different features between the WMS and the CS may possibly cause some deviations. Also, in the present work, the concentric annular flow was considered. This may be a good approximation for stable annular flows. However, it could give rise to some errors, specifically when the liquid-film distribution is significantly asymmetric and the unstable film is formed on the electrode walls. Although the measurement performance of the proposed sensor was fine overall compared to the WMS, its limitations observed in the experiments need to be further improved in future work.

In this study, an improved electrical-conductance sensor, which provided real-time information on the flow pattern and the void fraction, were applied to a horizontal pipe with a 40-mm inner diameter and a 5-m length. For several flow rate conditions covering stratified- and intermittent-flow regimes, the void fractions measured by the proposed sensor were compared with those of a WMS. The comparison results were overall in good agreement, however, due to difficulties in detecting the local phenomena in the proposed sensor, it generally showed underestimated values as compared to the WMS. Additionally, the concentric annular-flow assumption

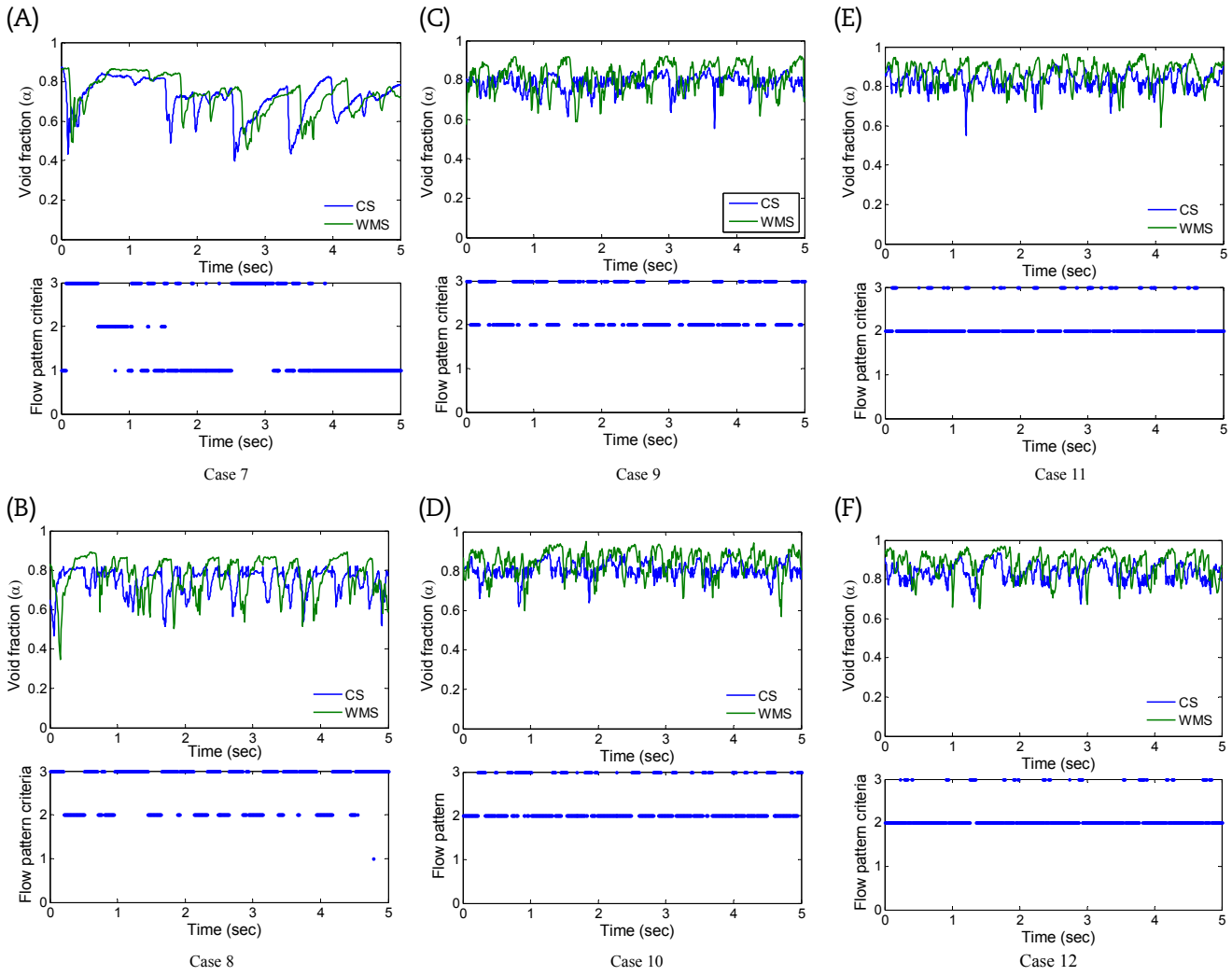


Fig. 12 – Comparison in instantaneous void fraction between CS and WMS for superficial gas velocities. The numbers '1', '2', and '3' on the y axis of the bottom figures represent the flow pattern criteria (7A), (7B), and (7C), respectively.

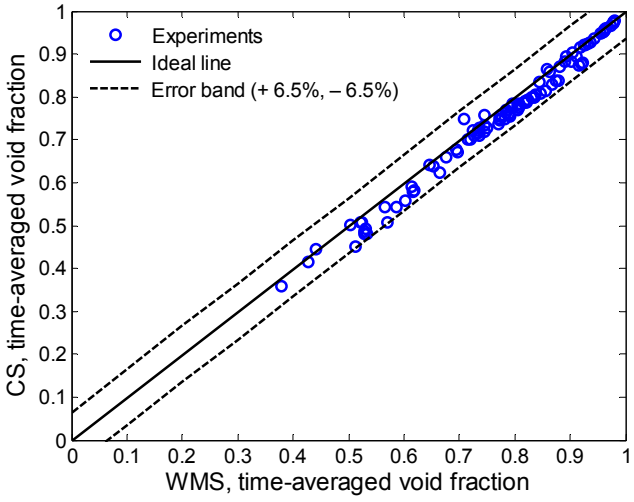


Fig. 13 – Comparison in time-averaged void fraction between CS and WMS.

used in the present work caused some deviations. This needs further improvement in future work. Nevertheless, the maximum deviation within 6.5% showed the feasibility of the proposed conductance sensor.

Conflicts of interest

All authors have no conflicts of interest to declare.

Acknowledgments

This work was supported by the Nuclear R&D Program (NRF-2012M2A8A4055548) and the Priority Research Centers Program (NRF-2010-0020077) through the National Research Foundation of Korea (NRF), funded by the Ministry of Education (MOE) and the Ministry of Science, ICT and Future Planning (MSIP) of the Korean government. Also, this work was supported by Chung-Ang University Research Grants received in 2014.

REFERENCES

[1] A.A. Kendoush, Z.A. Sarkis, Void fraction measurement by X-ray absorption, Exp. Therm. Fluid Sci. 25 (2002) 615–621.
[2] P. Stahl, P. Rudolf von Rohr, On the accuracy of void fraction measurements by single-beam gamma-densitometry for gas-liquid two-phase flows in pipes, Exp. Therm. Fluid Sci. 28 (2004) 533–544.
[3] J. Vejražka, M. Večeř, S. Orvalho, P. Sechet, M.C. Ruzicka, A. Cartellier, Measurement accuracy of a mono-fiber optical probe in a bubbly flow, Int. J. Multiph. Flow 36 (2010) 533–534.
[4] S. Paranjape, S.N. Ritchey, S.V. Garimella, Electrical impedance-based void fraction measurement and flow regime identification in microchannel flows under adiabatic conditions, Int. J. Multiph. Flow 42 (2012) 175–183.
[5] J.P. Schlegel, S. Miwa, M. Griffiths, T. Hibiki, M. Ishii, Development of impedance void meter for evaluation of flow symmetry, Ann. Nucl. Energy 63 (2014) 525–532.
[6] Z. Zhang, M. Bieberle, F. Barthel, L. Szalinski, U. Hampel, Investigation of upward cocurrent gas-liquid pipe flow using ultrafast X-ray tomography and wire-mesh sensor, Flow Meas. Instrum. 32 (2013) 111–118.
[7] R.E. Vieira, N.R. Kesana, B.S. McLaury, S.A. Shirazi, C.F. Torres, E. Schleicher, U. Hampel, Experimental investigation of the effect of 90° standard elbow on horizontal gas-liquid stratified and annular flow characteristics using dual wire-mesh sensors, Exp. Therm. Fluid Sci. 59 (2014) 72–87.
[8] D.C. Lowe, K.S. Rezkallah, Flow regime identification in microgravity two-phase flows using void fraction signals, Int. J. Multiph. Flow 17 (1999) 433–457.
[9] W.H. Ahmed, Capacitance sensors for void-fraction measurements and flow-pattern identification in air-oil two-phase flow, IEEE Sensors J. 6 (2006) 1153–1163.
[10] H. Canière, C. T'Joen, A. Willockx, M. De Paepe, Capacitance signal analysis of horizontal two-phase flow in a small diameter tube, Exp. Therm. Fluid Sci. 32 (2008) 892–904.
[11] S. Kim, J.S. Lee, K.Y. Kim, K.H. Kang, B.J. Yun, An approximate formula for the capacitance-void fraction relationship for annular flows, Meas. Sci. Technol. 20 (2009) 125404.
[12] K. De Kerpel, B. Ameel, S. De Schampheleire, C. T'Joen, H. Canière, M. De Paepe, Calibration of a capacitive void fraction sensor for small diameter tubes based on capacitive signal features, Appl. Therm. Eng. 63 (2014) 77–83.
[13] P. Andreussi, A. Di Donfrancesco, M. Messia, An impedance method for the measurement of liquid hold-up in two-phase flow, Int. J. Multiph. Flow 14 (1988) 777–785.
[14] N.A. Tsochatzidis, D.K. Karapantsios, M.V. Kostoglou, A.J. Karabelas, A conductance probe for measuring liquid fraction in pipes and packed beds, Int. J. Multiph. Flow 18 (1992) 653–667.
[15] M. Fossa, Design and performance of a conductance probe for measuring the liquid fraction in two-phase gas-liquid flows, Flow Meas. Instrum. 9 (1998) 103–109.
[16] J.R. Kim, Y.C. Ahn, M.H. Kim, Measurement of void fraction and bubble speed of slug flow with three-ring conductance probes, Flow Meas. Instrum. 20 (2009) 103–109.
[17] J.J.M. Geraets, J.C. Borst, A capacitance sensor for two-phase void fraction measurement and flow pattern identification, Int. J. Multiph. Flow 14 (1988) 305–320.
[18] J. Ye, L. Peng, W. Wang, W. Zhou, Optimization of helical capacitance sensor for void fraction measurement of gas-liquid two-phase flow in a small diameter tube, IEEE Sensors J. 11 (2011) 2189–2196.
[19] H.C. Yang, D.K. Kim, M.H. Kim, Void fraction measurement using impedance method, Flow Meas. Instrum. 14 (2003) 151–160.
[20] S. Huang, X. Zhang, D. Wang, Z. Lin, Equivalent water layer height (EWLH) measurement by a single-wire capacitance probe in gas-liquid flows, Int. J. Multiph. Flow 34 (2008) 809–818.
[21] D. Barnea, Transition from annular flow and dispersed bubble flow – unified models for the whole range of pipe inclinations, Int. J. Multiph. Flow 12 (1986) 733–744.
[22] M.S. Ko, B.J. Yun, K.Y. Kim, S. Kim, Design of a capacitance sensor for void fraction measurement in annular flows through a vertical pipe, Meas. Sci. Technol. 23 (2012) 105301.
[23] Y. Taitel, A.E. Dukler, A model for predicting flow regime transitions in horizontal and near horizontal gas-liquid flow, AICHE J. 22 (1976) 47–55.
[24] H.M. Prasser, A. Bottger, J. Zschau, A new electrode-mesh tomograph for gas-liquid flows, Flow Meas. Instrum. 9 (1998) 111–119.
[25] J.M. Mandhane, G.A. Gregory, K. Aziz, A flow pattern map for gas–liquid flow in horizontal pipes, Int. J. Multiph. Flow 1 (1974) 537–553.